

## **A weather regime characterisation of winter biomass aerosol transport from southern Africa**

Marco Gaetani (1,2); Benjamin Pohl (3); Maria del Carmen Alvarez Castro (4,5); Cyrille Flamant (6); Paola Formenti (1)

(1) Institut Pierre Simon Laplace, Laboratoire Interuniversitaire des Systèmes Atmosphériques, UMR CNRS 7583, Université Paris-Est Créteil, Université de Paris, Institut Pierre Simon Laplace, Créteil, France

(2) Scuola Universitaria Superiore IUSS, Pavia, Italia

(3) CRC/Biogéosciences, UMR6282 CNRS / Université de Bourgogne Franche-Comté, Dijon, France

(4) University Pablo de Olavide, Seville, Spain

(5) CMCC, Bologna, Italy

(6) Institut Pierre Simon Laplace, Laboratoire Atmosphères, Milieux, Observations Spatiales, UMR CNRS 8190, Sorbonne Université, Université Versailles Saint Quentin, Paris, France

Contact: [marco.gaetani@iusspavia.it](mailto:marco.gaetani@iusspavia.it)

### **Supplement**

#### **S1. PCA analysis and class partition**

The daily variability of the atmospheric circulation over southern Africa and the South Atlantic in ASO is analysed in terms of EOFs of the geopotential height at 700 hPa, which show the first 2 modes accounting for 58.4% of the total variability (Fig. S1ab). The positive phase of the first EOF (which explains 31.7% of the variability) is characterised by a high pressure anomaly dominating southern Africa and a low pressure anomaly in the South Atlantic (Fig. S1a). The associated circulation anomaly is favourable to BBA transport from tropical southern Africa towards the Atlantic and a recirculation southward along the Namibian coast, while the transport from South Africa towards the Indian Ocean is inhibited (Fig. S1a). The positive phase of the second EOF (explaining 26.7% of the variability) shows a high pressure anomaly dominating the circulation over southern Africa and South Atlantic, pushing the northerly BBA recirculation westward over the South Atlantic and further weakening the transport towards the Indian Ocean (Fig. S1b). The first two EOFs explain similar variance and show similar spatial patterns shifted in the longitudinal dimension, suggesting that they form a pair in quadrature. This hypothesis is tested by computing the daily lead/lag correlation between the first PC time series (PC1) and itself, to be compared with the lead/lag correlation between PC1 and PC2 (Fig. S2). The maximum correlation between PC1 and PC2 is 0.34 at a lead time of 2 days. Synoptic centres of action in EOF1 and 2 are shifted by about 14-20° in longitude (Fig. S1ab), so given the 2-day lag between the positive phase of EOF1 and 2, the apparent propagation speed is 7-10°/day eastwards, i.e. 7.0-9.6 m/s (at 40°S, 1° in longitude equals 85 km). Considering that the mean zonal flow at 700 hPa in ASO in the

35-40°S belt in the South Atlantic is 12.8 m/s, these values are consistent with travelling Rossby waves with wave number 8-12. Therefore, these two circulation modes represent the variability associated with high-wave-number propagative disturbances along the midlatitude westerly flow (see e.g. Widlansky et al. [2011] and van der Wiel et al. [2015] for the characterisation of synoptic disturbances in southern midlatitudes). The third EOF (explaining 14.1% of the variability) is also associated with a circulation pattern resembling to a wave pattern displaced along the midlatitude mean flow, which modulates the meridional recirculation of BBA poleward (Fig S1c). The fourth EOF (explaining 8.1%) is characterised by the variability of the pressure in the South Atlantic, which modulates the midlatitude westerly flow and the westward BBA transport in the Tropics (Fig. S1d).

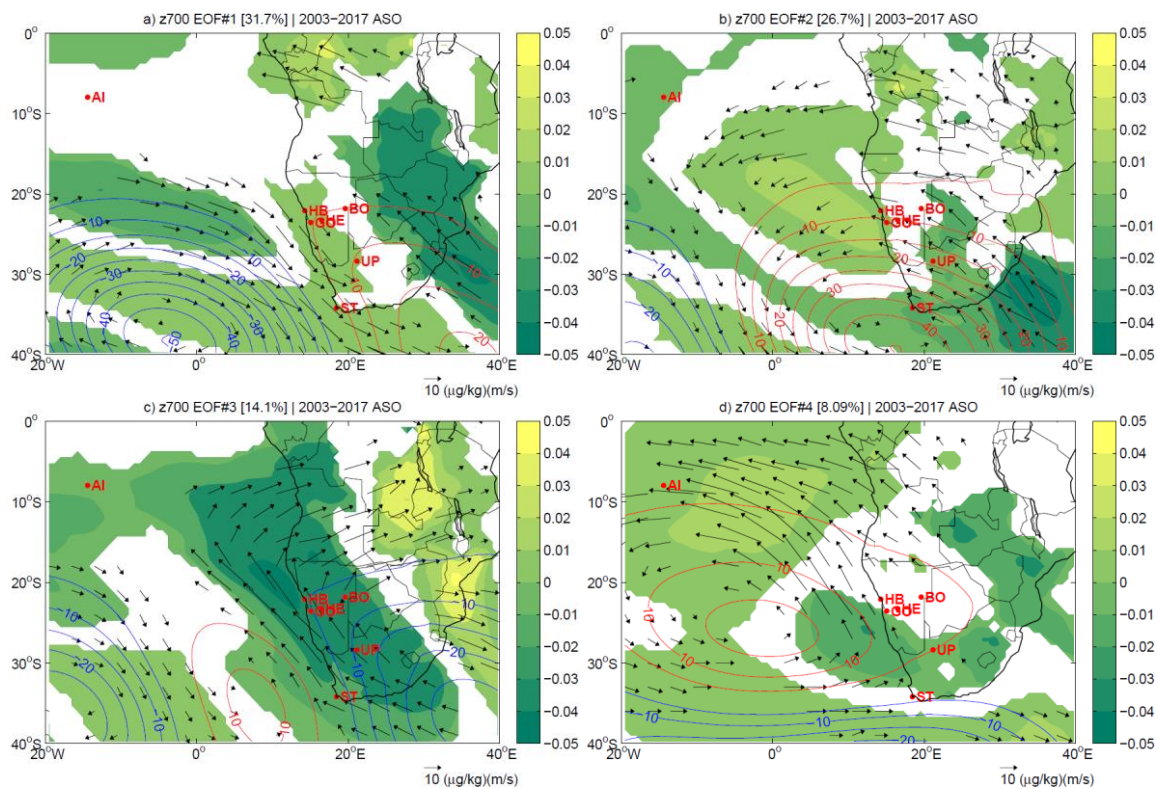


**Figure S1.** Anomaly patterns of CAMS geopotential height (m, contours), AOD at 550 nm (shadings) and BBA transport (( $\mu\text{g}/\text{kg}$ )(m/s), arrows) at 700 hPa associated with the first to fourth EOF of the geopotential height at 700 hPa in ASO 2003-2017 (EOF explained variance is displayed in brackets). Anomaly patterns are computed by regressing daily anomaly data onto standardised time series derived from the PCA; only values significant at 95% level of confidence are displayed; red dots indicate the locations of the AERONET stations (main text, Table 1).

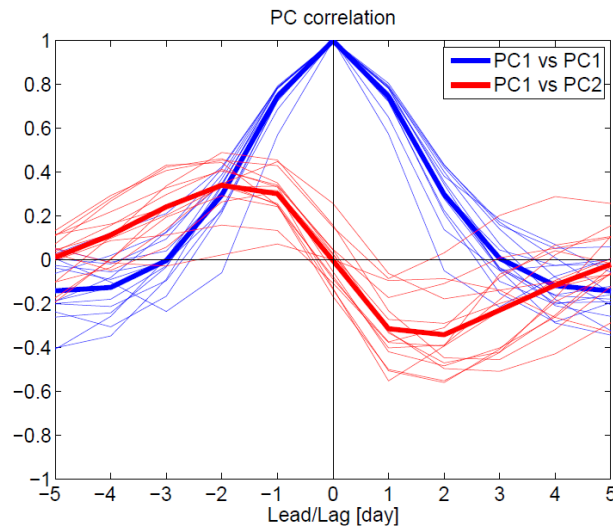


**Figure S2.** Daily lead/lag correlation of PC1 with itself (in blue) and PC1 with PC2 (in red): thin lines represent the correlation in individual years, thick lines represent the 2003-2017 average.

The first 4 EOFs, accounting for 80% of total variability, are used to filter out the noise associated with the lowest rank modes from daily variability, which is then classified into circulation types by means of a k-means algorithm, using  $k = [2, 10]$  (Michelangeli et al., 1995). For each  $k$ , the classification is performed 100 times, to ensure reproducibility of the results. A red-noise test is performed to assess the significance of the class partition (Michelangeli et al., 1995), resulting in 6 and 7 classes (Fig. S3). The synoptic characterisations of the BBA transport performed by using 6 and 7 classes are presented in the main text and in following Section S2, respectively.

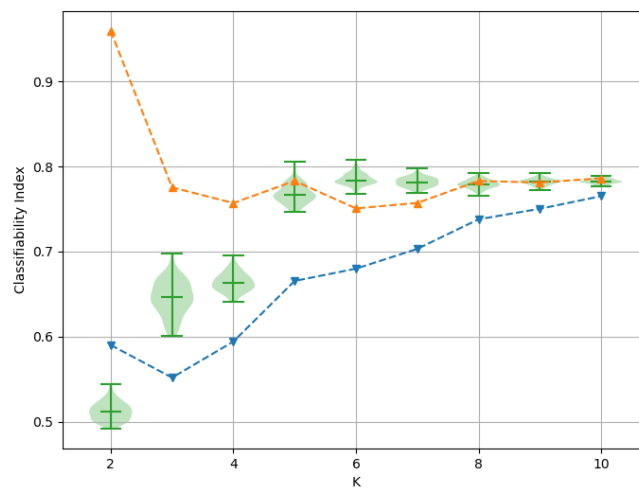


**Figure S3.** Spread of the classificability index (violin plots) as a function of the number of regimes ( $K$ ) for 100 clusterings initialized with different random draws. The levels of significance at 5 and 95% (blue line and orange line, respectively) are computed according to a first-order Markov process (also known as “red-noise test”).

## S2. WR classification (7 classes) and BBA transport characterisation

The WR classification shows a circulation anomaly associated with a strengthening of the continental high (WR1), resulting from the westward extension of the Mascarene High (Fig. S4a). This WR occurs at a frequency of 13.7%, which is almost constant during the season (Fig. S5). The occurrence of WR1 increases BBA transport above Ascension Island, but has little impact on continental stations, with the exception of the Simon's Town station, where the anomalous transport seems related to increased transport from South America by reinforced midlatitude westerlies (Chazette et al., 2019) (Fig. S4a). Two synoptic patterns (WR5 and 7) account for the oscillation of the pressure field in the South Atlantic (Fig. S4). This synoptic variability is dominated by the WR7, which occurs at a frequency of 18.9% and is characterised by a high pressure anomaly in the South Atlantic accompanied by a reinforcement of the midlatitude westerlies (Fig. S4g). Its symmetric counterpart is represented by WR5, which occurs at a frequency of 15.2% and is characterised by a low pressure anomaly and a weaker westerly flow in the midlatitudes (Fig. S4e). WR7 occurs mainly in September-October, while WR5 is less frequent in September (Fig. S5). The occurrence of these WRs is associated with the modulation of BBA transport above the South Atlantic, and have limited impact over the continent. Four synoptic patterns (WR2, 3, 4 and 6) represent the fingerprint of midlatitude disturbances propagating along the westerly flow, and account for 51.9% of the synoptic variability (Fig. S4). The frequency of WR2 and 3 decreases during the season, while WR4 and 6 show the opposite tendency (Fig. S5). These WRs are characterised by the longitudinal displacement of high-low pressure anomalies modulating the meridional circulation, which in turn drives the poleward BBA transport above the South Atlantic and southern Africa. In particular, WR2 favours the recirculation of BBA from the ocean towards Namibia and South Africa, leading to significant positive AOD anomalies above the continental stations (Fig. S4b), while WR6 pushes the BBA recirculation above the South Atlantic, resulting in significant positive AOD anomalies above coastal stations, and inhibits the BBA transport towards the Indian Ocean (Fig. S4f). Conversely, WR3 and 4 inhibit the BBA recirculation, leading to significant negative AOD anomalies the continental stations (Fig. S4c,d).

The circulation-to-environment (C2E) characterisation of the AOD AERONET station data (for details, see Section 2.3 and Table 1 in the main text) is presented in Fig. S6 and Table S1. At Ascension Island station, AOD anomalies during WR5 show a preference for negative values (Fig. S6a). The significance of this characterisation is confirmed by the ANOVA with a level of confidence higher than 99%. Just south of the source region, AOD anomalies in Bonanza do not show any preference for different WRs, as also confirmed by ANOVA ( $p=0.37$ ) indicating no significance for this characterisation. In central Namibia, in Gobabeb, Henties Bay and HESS negative AOD anomalies are associated with WR3 and 4 (Fig. S6c-e). Moreover, WR2 and 5 are associated with positive anomalies in HESS and Gobabeb, respectively (Fig. S6c,e). Interestingly, WR5 is associated with significant AOD anomalies not showing a preferred sign (Fig. S6e). In this case, the KS test account for the differences in the shape of the distributions rather than in the mean. For these stations, the ANOVA indicates that the characterisation is significant with a level of confidence higher than 99%. Similarly, the continental station in Upington shows positive anomalies associated with WR2, while WR3 and 4 leads to negative anomalies (Fig. S6g). The ANOVA indicates that the characterisation is significant ( $p=0.05$ ) in this location. In South Africa, the southernmost station in Simon's Town the WR characterisation is poor ( $p=0.09$ ) and no significant anomalies are associated with any WR (Fig. S6f).

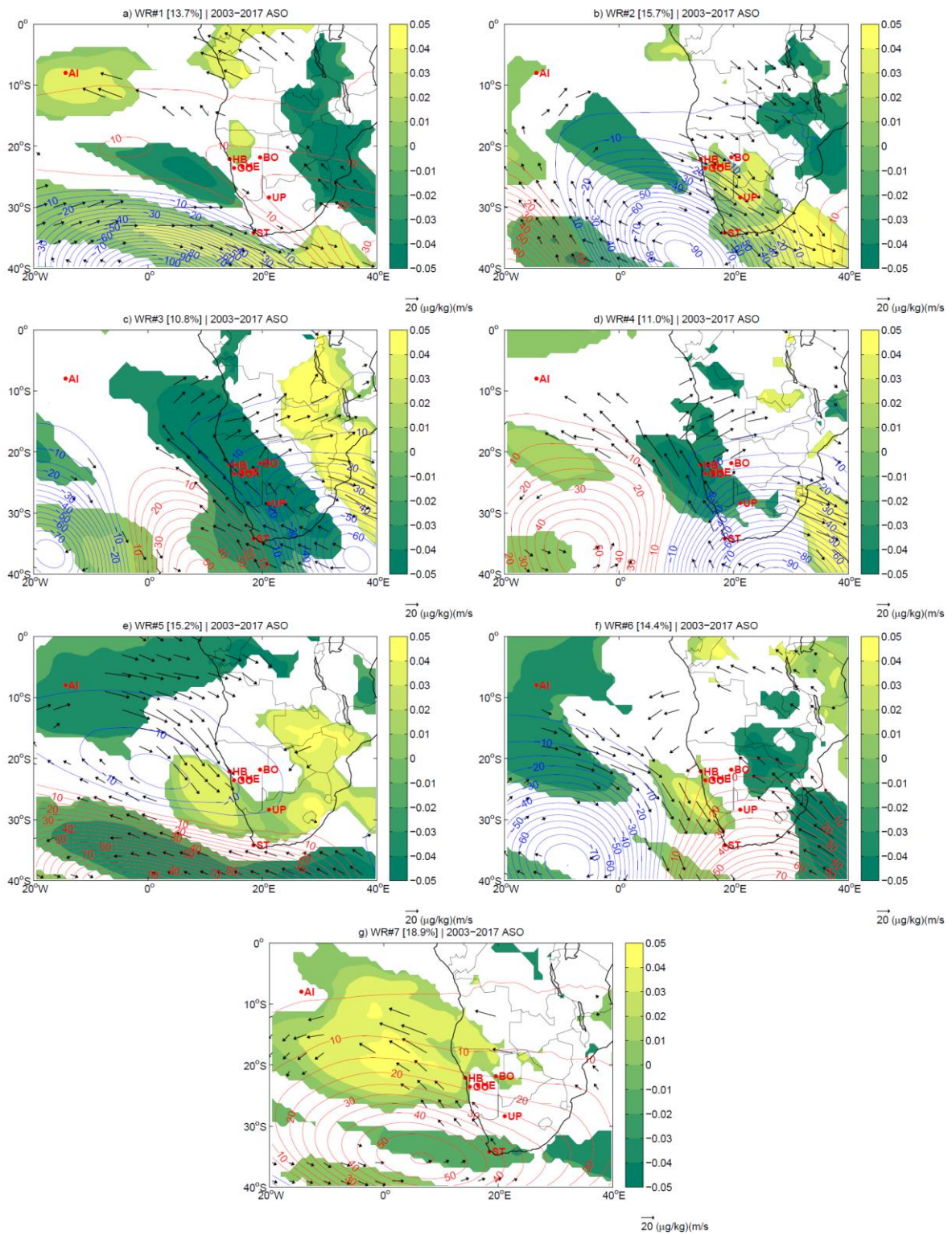


**Figure S4.** Anomaly patterns of CAMS geopotential height (m, contours), AOD at 550 nm (shadings) and BBA transport (( $\mu\text{g}/\text{kg}$ )(m/s), arrows) at 700 hPa associated with the WRs classified from the geopotential height at 700 hPa in ASO 2003-2017. Frequency of the WRs is indicated in brackets; only values significant at 95% level of confidence for a Student's t-test are displayed.

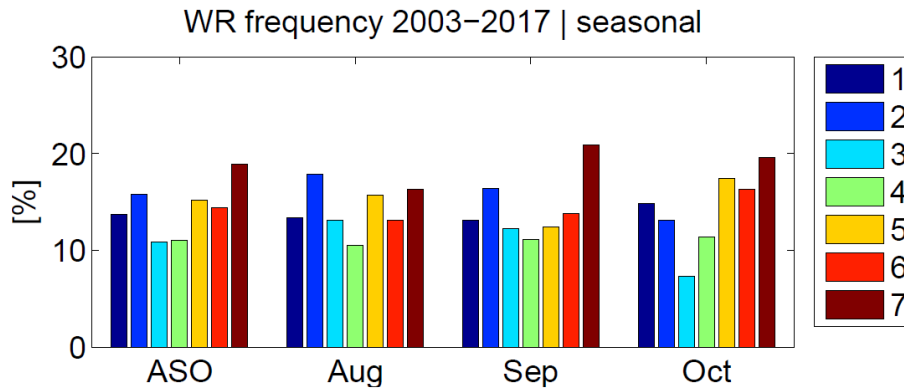


**Figure S5.** WR frequency 2003-2017: seasonal and monthly.

**Table S1.** P-values of ANOVA and Kolmogorov-Smirnov test. Values lower than 0.05 are reported in bold.

Station	ANOVA	WR1	WR2	WR3	WR4	WR5	WR6	WR7
Ascension Island (AI)	<b>&lt;0.01</b>	0.16	0.51	0.78	0.23	<b>0.01</b>	0.91	0.53
Bonanza (BO)	0.37	0.82	0.90	0.13	0.27	0.18	0.95	0.43
Gobabeb (GO)	<b>&lt;0.01</b>	0.89	0.65	<b>0.03</b>	<b>&lt;0.01</b>	<b>&lt;0.01</b>	0.98	0.76
Henties Bay (HB)	<b>&lt;0.01</b>	0.22	0.95	<b>0.02</b>	<b>0.04</b>	0.13	0.55	0.92
HESS (HE)	<b>&lt;0.01</b>	0.51	<b>0.01</b>	<b>0.05</b>	0.13	<b>0.03</b>	0.61	0.45
Simon's Town IMT (ST)	0.09	0.17	0.58	0.12	0.97	0.53	0.49	0.18
Upington (UP)	<b>0.05</b>	0.88	<b>&lt;0.01</b>	0.07	<b>0.01</b>	0.40	0.13	0.91

The environment-to-circulation (E2C) characterisation of the AOD AERONET station data (for details, see Section 2.3 and Table 1 in the main text) is presented in Fig. S7 and Table S2. In Ascension Island, positive AOD anomalies are accompanied by an increase in the occurrence of WR2 and 4, while negative anomalies are associated with more frequent WR3 and 5 (Fig. S7a). The Bonanza station does not show any significant change in the WR occurrence. Central Namibia stations in Gobabeb, Henties Bay and HESS show positive AOD anomalies associated with more frequent WR1, 2 and 5, while negative anomalies are accompanied by increased occurrence of WR3 and 4 (Fig S7c-e). However, in HESS increased occurrence of WR5 is also associated with negative anomalies for WR5. Similarly, in Upington increased occurrence of WR2 and 5 is associated with positive AOD anomalies, while more frequent WR4 and 5 are associated with negative anomalies (Fig. S7g). In Simon's Town, increased occurrence of WR1, 5 and 6 is associated with positive AOD anomalies (Fig. S7f). The ambiguity in the association of WR5 to both positive and negative AOD anomalies may be explained by the location of the continental stations at the margin of the BBA transport path (Fig. S4e), making them highly sensible to the variability of the circulation around the centroid.

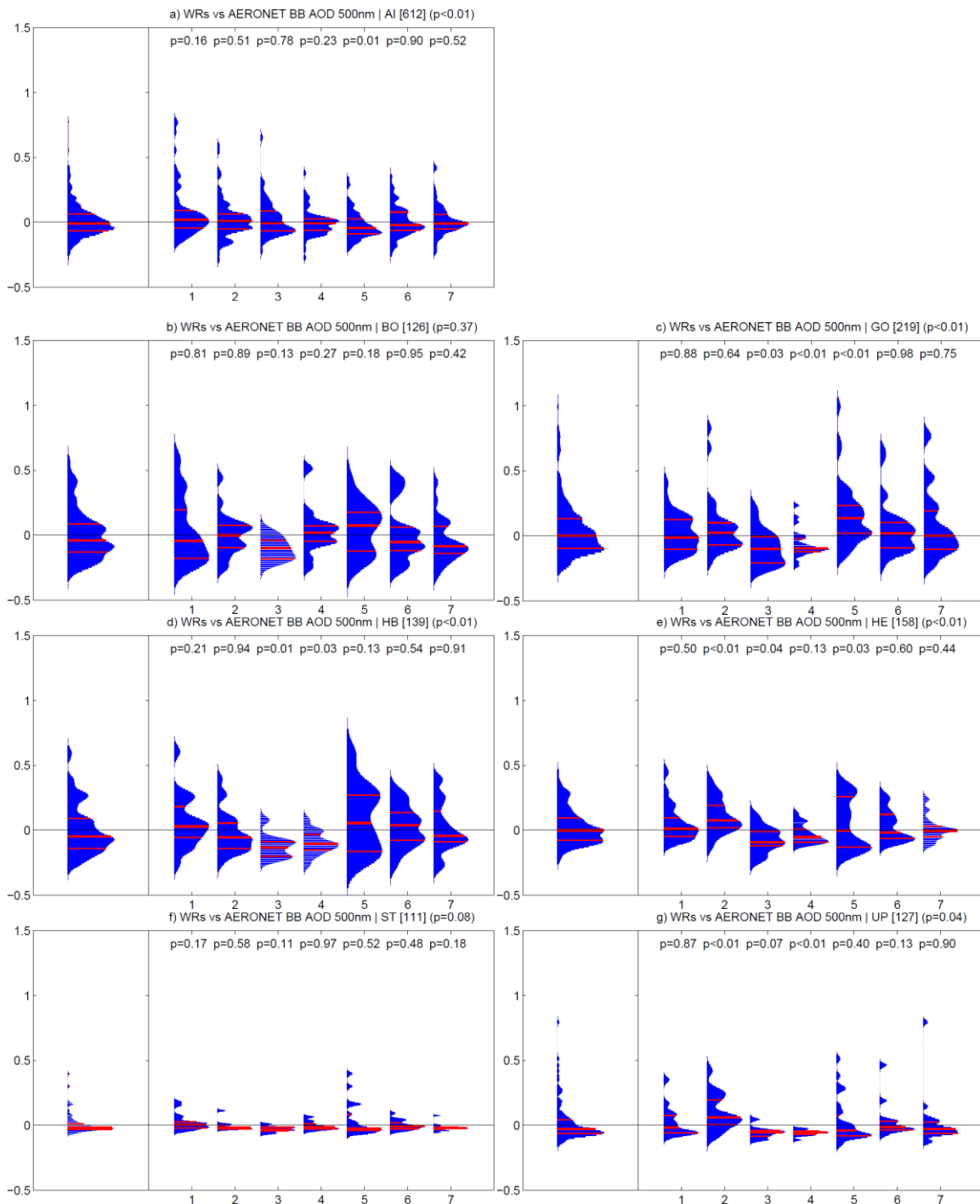


**Figure S6.** Circulation-to-environment characterisation: distributions of the AOD anomalies at 500 nm at the AERONET stations (main text, Table 1), and as a function of the WRs. Probability density functions are estimated by using a normal kernel density; red lines represent 25th, 50th and 75th percentiles. For each WR, the p-value of a Kolmogorov-Smirnov test used to assess the difference with the total sample is reported. In titles, in brackets the number of available daily observations and the p-value of the ANOVA used to assess the WR characterisation are reported.

**Table S2.** Environment-to-circulation characterisation: Chi-squared statistics for each quartile (Q1-4) at the AERONET stations (Table 1). Values exceeding 12.59, i.e. the critical threshold for the Chi-squared distribution with 6 degrees of freedom at 95% level of confidence, are reported in bold.

Station	Q1	Q2	Q3	Q4
Ascension Island (AI)	<b>14.01</b>	4.87	<b>13.04</b>	11.69
Bonanza (BO)	1.28	3.28	6.68	9.80
Gobabeb (GO)	<b>14.55</b>	3.56	9.01	<b>25.43</b>
Henties Bay (HB)	5.44	6.83	3.91	<b>17.12</b>
HESS (HE)	<b>16.35</b>	8.09	9.61	<b>13.63</b>
Simon's Town IMT (ST)	8.10	2.01	4.62	<b>19.09</b>
Uppington (UP)	<b>17.13</b>	9.08	7.80	<b>15.64</b>

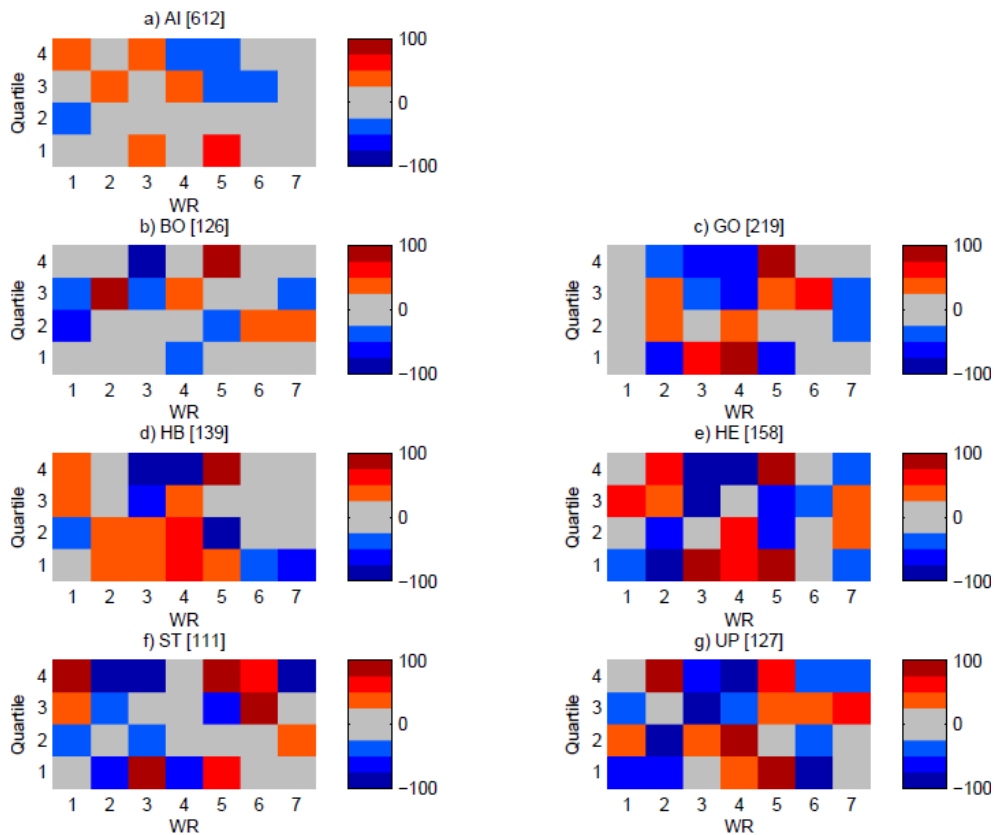


**Figure S7.** Environment-to-circulation characterisation: WR frequency anomaly as a function of the quartiles of the AOD anomalies at 500 nm at the AERONET stations (main text, Table 1). Values are percentage changes relative to climatological frequencies. In brackets, the number of available daily observations are indicated.

The WR frequency in ASO is analysed at the interannual time scale. No significant trend is found in the WR occurrence after a Mann-Kendall test at 95% level of confidence, with the exception of WR5, showing an increasing trend in the 2003-2017 period (Fig. S8). However, the limited time coverage of the time series prevents the robust assessment of the statistical significance of the detected trends. All the WRs show similar interannual variability in the frequency of occurrence (2-5% standard deviation) (Fig. S8). Possible teleconnections controlling the WR interannual variability are analysed by computing the linear correlation between the WR frequency and the SST variability at the global scale (Fig. S9). WRs characterised by circulation patterns describing travelling disturbances (WR2, 3, 4

and 6) show no significant correlations at the global scale, with the exception of localised SST anomalies in the South Atlantic. WR3 also shows SST anomalies in the eastern Indian Ocean and the western Pacific, and WR4 also shows SST anomalies in the Southern Ocean. WR7 shows a strong relationship with El Niño/Southern Oscillation (ENSO)-like patterns. In particular, WR7 occurrence is associated with La Niña conditions (Fig. S9g). The linkage with La Niña conditions explains the peak in 2010 associated with a strong La Niña event (Boening et al., 2012), and the minimum in 2015, associated with an extreme El Niño event (Hu and Fedorov, 2017). The comparison of the correlation analysis performed using HadISST and NOAA ERSST data show only minor differences (cf. Fig. S9 and Fig. S10). The analysis of the WR correlation with the geopotential at 200 hPa (Fig. S11) shows a tropics-extratropics wave pattern connecting the Pacific to South Atlantic for WR7, highlighting the ENSO teleconnection. Weakly significant correlation patterns are also found at mid-to-high latitudes for WR1-6, suggesting a possible connection with the Southern Annular Mode variability (see Pohl and Fauchereau (2012)).

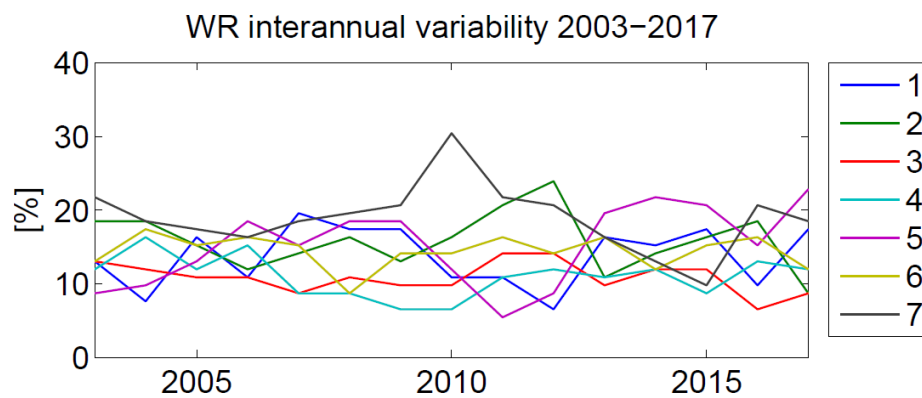


**Figure S8.** WR frequency 2003-2017: interannual variability.

The impact of the WR interannual variability on the BBA transport is assessed by computing the linear correlation with the CAMS AOD at 550 nm and the BBA transport at 700 hPa (Fig. S12). The WR variability affects the mid-tropospheric circulation in the subtropics, modulating the BBA transport on both the zonal and the meridional direction. However, the correlation analysis reveal that the WR variability has weak impact on the BBA transport at the interannual time scale, with only three WRs controlling the BBA transport in the region. Specifically, WR4 inhibits the BBA transport above Tropical Atlantic and the recirculation towards southern Africa (Fig. S12d); WR6 favours the BBA recirculation in the South Atlantic (Fig. S12f); and WR7 favours the recirculation of BBA towards southern Africa (Fig. S12g).

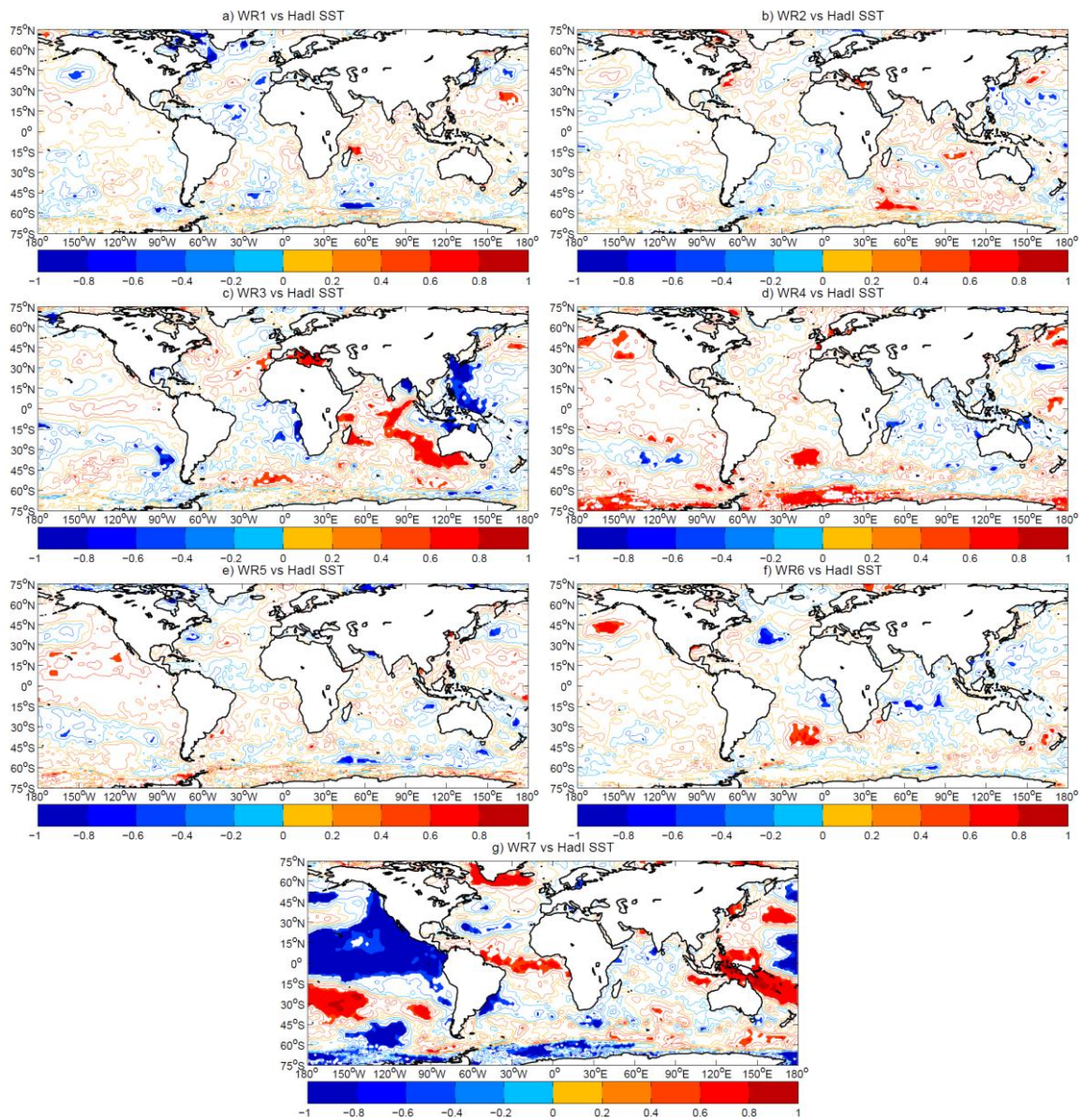


**Figure S9.** Interannual correlation over the period 2003-2017: WR frequency vs Hadl SST in ASO. Shadings display significant correlations at 95% level of confidence. Time series are detrended and standardised.

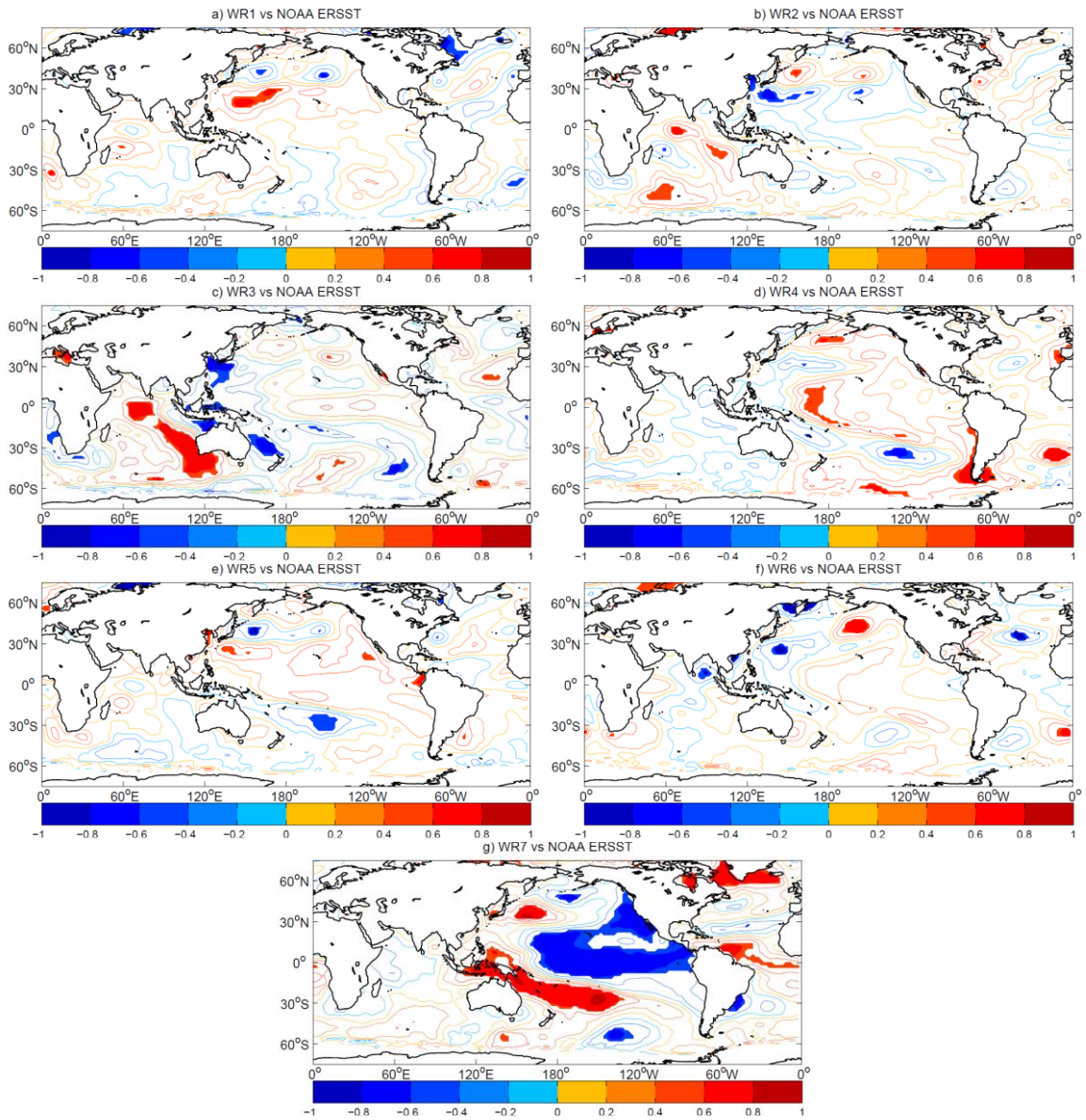


**Figure S10.** Interannual correlation over the period 2003-2017: WR frequency ( $k=7$ ) vs NOAA SST in ASO. Shadings display significant correlations at 95% level of confidence. Time series are detrended and standardised.

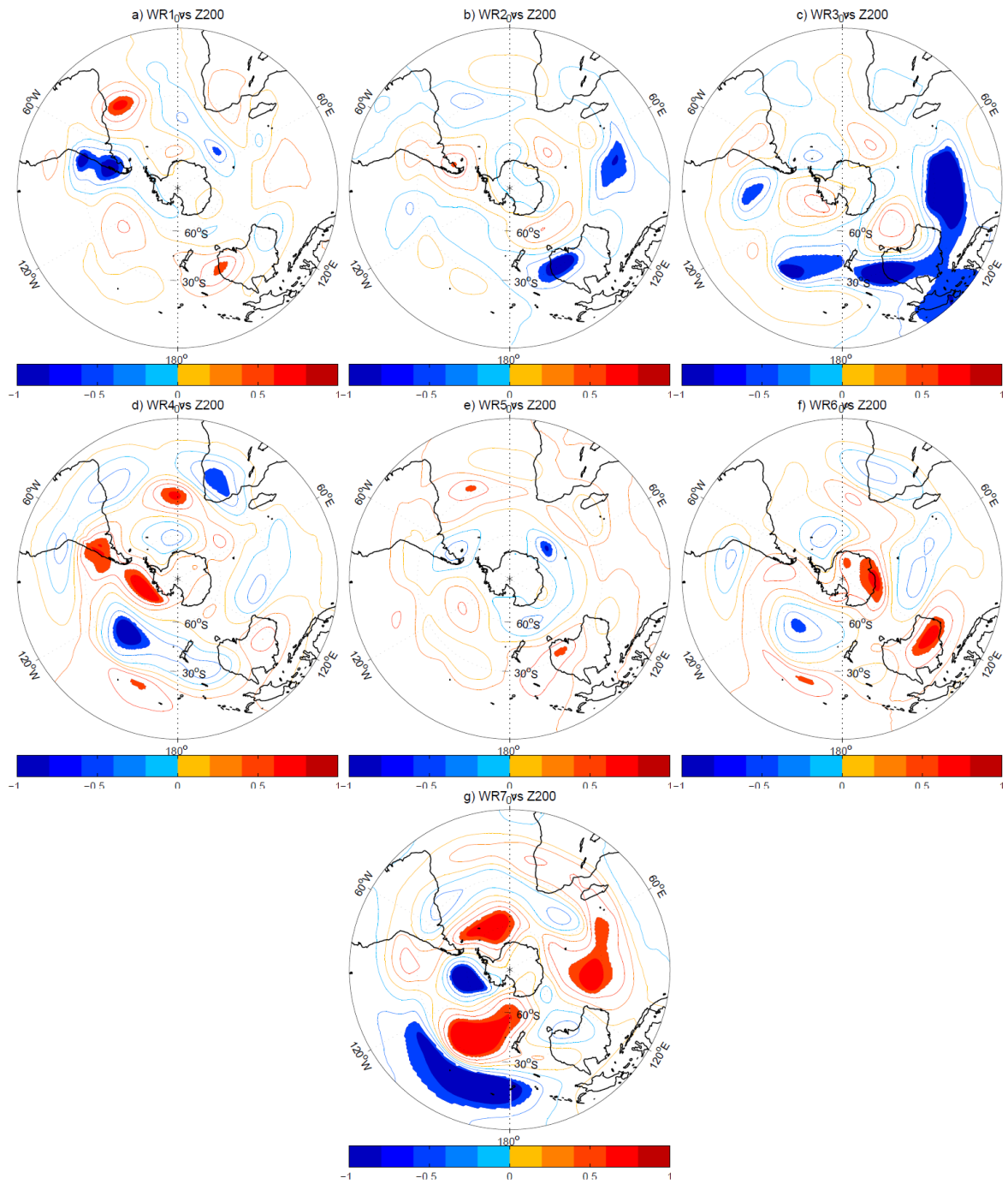


**Figure S11.** Interannual correlation over the period 2003-2017: WR7 frequency vs geopotential at 200 hPa in ASO. Shadings display significant correlations at 95% level of confidence. Time series are detrended and standardised.

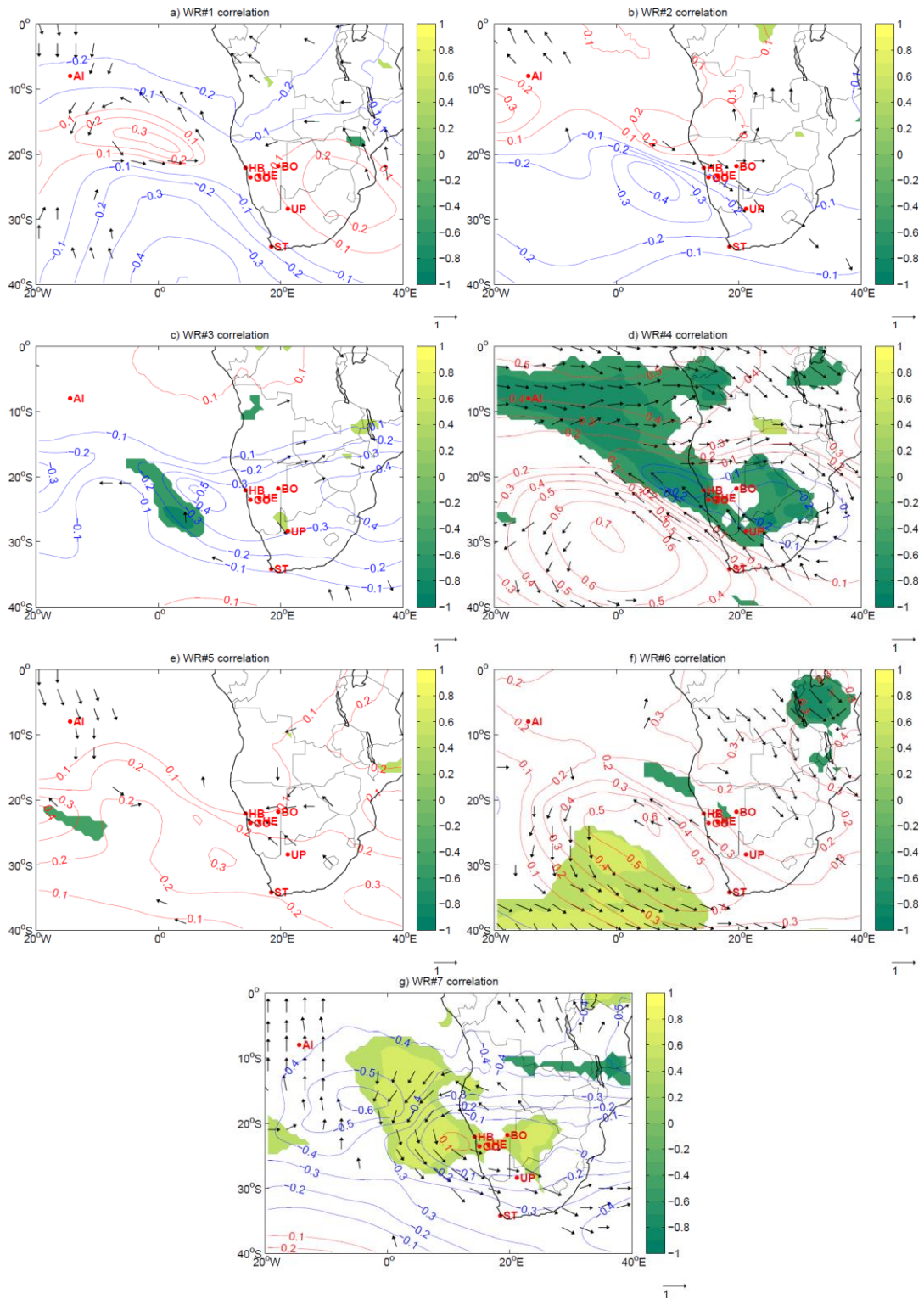


**Figure S12.** Correlation maps of WR frequency vs CAMS geopotential height (contours), AOD at 550 nm (shadings) and BBA transport (arrows) at 700 hPa. For AOD and BBA transport only correlation significant at 95% level of confidence are displayed. Data are detrended and standardised.

### S3. WR-SST interannual teleconnection (k=6, NOAA SST data)

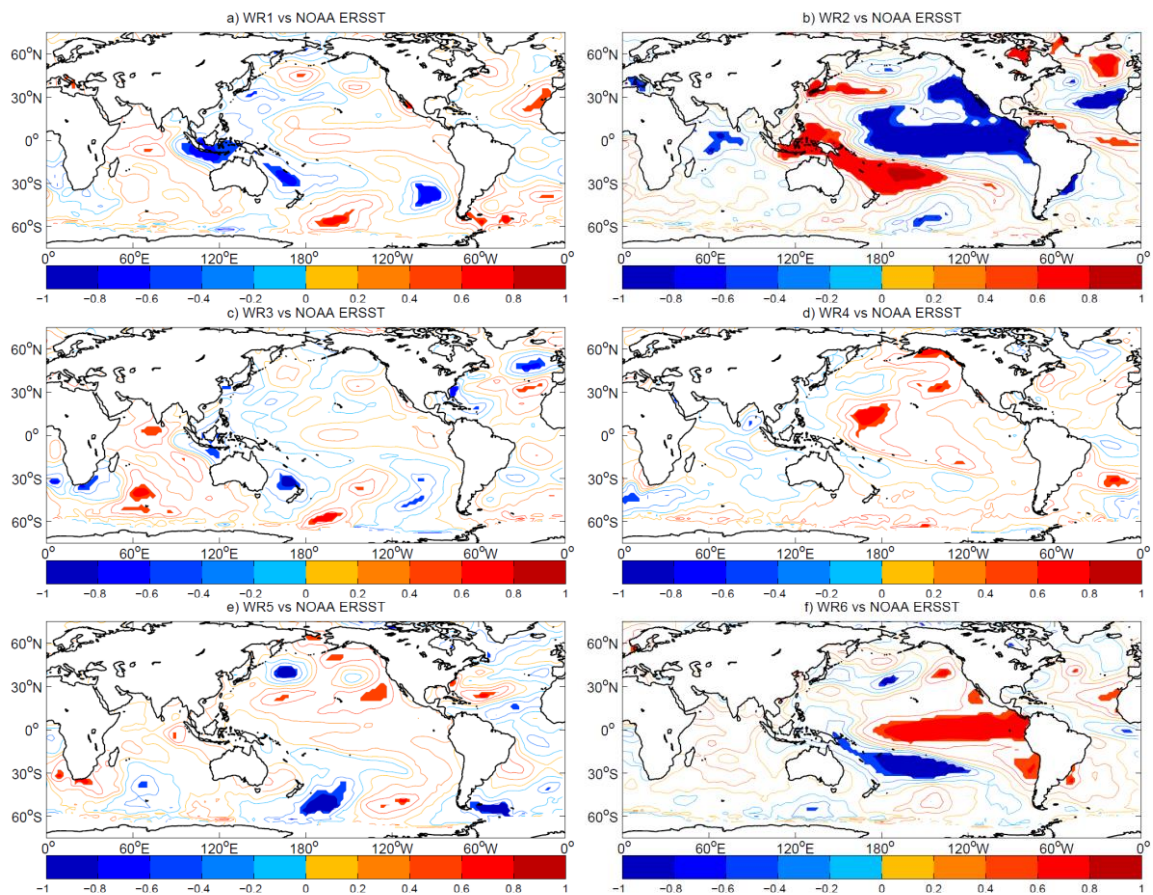


**Figure S13.** Interannual correlation over the period 2003–2017: WR frequency (k=6) vs NOAA SST in ASO. Shadings display significant correlations at 95% level of confidence. Time series are detrended and standardised.

### References

- Boening, C., Willis, J. K., Landerer, F. W., Nerem, R. S. and Fasullo, J.: The 2011 La Niña: So strong, the oceans fell, *Geophys. Res. Lett.*, 39(19), n/a-n/a, doi:10.1029/2012GL053055, 2012.
- Chazette, P., Flamant, C., Totems, J., Gaetani, M., Smith, G., Baron, A., Landsheere, X., Desboeufs, K., Doussin, J.-F. and Formenti, P.: Evidence of the complexity of aerosol transport in the lower troposphere on the Namibian coast during AERO-CLO-sA, *Atmos. Chem. Phys.*, 19(23), 14979–15005, doi:10.5194/acp-19-14979-2019, 2019.
- Hu, S. and Fedorov, A. V.: The extreme El Niño of 2015–2016 and the end of global warming hiatus, *Geophys. Res. Lett.*, 44(8), 3816–3824, doi:10.1002/2017GL072908, 2017.
- Michelangeli, P. A., Vautard, R. and Legras, B.: Weather regimes: recurrence and quasi stationarity, *J. Atmos. Sci.*, 52(8), 1237–1256, doi:10.1175/1520-0469(1995)052<1237:WRRRAQS>2.0.CO;2, 1995.
- Pohl, B. and Fauchereau, N.: The southern annular mode seen through weather regimes, *J. Clim.*, 25(9), 3336–3354, doi:10.1175/JCLI-D-11-00160.1, 2012.
- Widlansky, M. J., Webster, P. J. and Hoyos, C. D.: On the location and orientation of the South Pacific Convergence Zone, *Clim. Dyn.*, 36(3), 561–578, doi:10.1007/s00382-010-0871-6, 2011.

van der Wiel, K., Matthews, A. J., Stevens, D. P. and Joshi, M. M.: A dynamical framework for the origin of the diagonal South Pacific and South Atlantic Convergence Zones, *Q. J. R. Meteorol. Soc.*, 141(691), 1997–2010, doi:10.1002/qj.2508, 2015.